Langmuir

Article

pubs.acs.org/Langmuir

Gravity and Surface Tension Effects on the Shape Change of Soft Materials

Xuejuan Xu,[†] Anand Jagota,[∥] Songming Peng,[‡] Dan Luo,[‡] Mingming Wu,[‡] and Chung-Yuen Hui*[,§]

[†]Sibley School of Mechanical and Aerospace Engineering, [‡]Department of Biological and Environmental Engineering, and [§]Field of Theoretical and Applied Mechanics, Cornell University, Ithaca, New York 14853, United States

[∥]Department of Chemical Engineering, Lehigh University, Bethlehem, Pennsylvania 18015, United States

Supporting Information

ABSTRACT: Surface tension and gravity, whose influence on the deformation of conventional engineering materials is negligible, become important for soft materials that are typically used in the microfabrication of devices such as microfluidic channels. Although for soft materials the shape change due to these forces can be large, it is often neglected in the design processes. To capture conditions under which the influence of these forces is important, we propose a deformation map in which the shape change is captured by two dimensionless material parameters. Our idea is demonstrated by simulating the large deformation of a short circular cylinder made of a neo-Hookean material in frictionless contact with a rigid substrate. These simulations are carried out using a finite element model that accounts for surface tension and gravity. Our model integrates the two different approaches typically used to determine the shape change of solids and liquid drops in contact with a substrate.

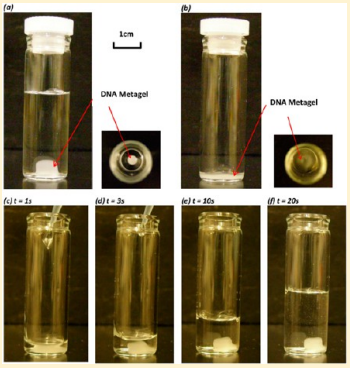

1. INTRODUCTION

Soft materials such as elastomers and hydrogels can support very large deformation and play an increasingly important role in engineering applications. Poly(dimethylsiloxane) (PDMS), for example, is often used for stamps in micro- and nanoprinting for its low surface energy, transparency, and elasticity.[1] It can also be used as a mold to transfer or replicate surface patterns from hard substrates. Such pattern transfer is important for many applications such as microfluidic devices[2] and bioinspired adhesives.[3] A different class of soft materials consists of hydrogels, which are essentially polymer networks swollen in water. The biocompatibility of many hydrogels and their ability to respond to environmental stimuli make them attractive candidates for many biological and engineering applications such as bioseparation, drug delivery, and tissue scaffolding.[4]

The Young's modulus of most elastomers is on the order of megapascals. For hydrogels, this number ranges from hundreds to thousands of pascals. Most notably, a recent development in synthetic hydrogels has led to the creation of a highly stretchable DNA hydrogel (metagel) with a modulus on the order of only a few pascals.[5] Traditionally, engineering analysis of the deformation of solids neglects the influence of surface tension and gravity. (Gravity loading is important for very large structures such as buildings and dams.) In his article on surface tension, Gibbs[6] in 1876 stated that "the rigidity of solids is in general so great, that any tendency of the surfaces of discontinuity to variation in area or form may be neglected in comparison with the forces which are produced in the interior of solids by any sensible strains, so that it is not necessary to take account of the surface of discontinuity in determining the state of strain of solid masses". However, for very soft materials, surface tension can be the dominant driving force of shape change. Figure 1a shows an image of a DNA metahydrogel in water after being released from its cylindrical mold. Because the gel consists mostly of water, the loading due to gravity and surface tension is relatively small when the gel is submerged in water; therefore, it retains its (cylindrical) shape. However, when water is drained from the container, it immediately deforms to a pancake shape by the dual action of gravity and surface tension; its original shape is unrecognizable (Figure 1b). Remarkably, because of its elasticity, it recovers to its original shape in Figure 1c–f when water is reintroduced. This memory effect is due to elasticity and not to changes in microstructure. A less dramatic example of surface-induced shape change can be found in the microfabrication of PDMS stamps. The corners of PDMS stamps released from silicon molds are never as sharp as the molds, suggesting that surface tension has caused the rounding of these corners.[1] Recently, Jagota et al.[7] have shown that a gel replica of a rippled PDMS master has a much reduced amplitude (about a 60% reduction). The influence of the liquid surface tension on the deformation of solids has been studied extensively in recent years.[8] An important example is the deformation of a substrate due to forces at the triple line of a drop on a substrate,[9] where the additional role of solid–fluid surface tension has recently been established.[10] Clearly, the role of surface tension and gravity on the shape of structures will become more significant as the modulus decreases.[11,12]

Received: March 11, 2013
Revised: May 1, 2013
Published: June 10, 2013

   dx.doi.org/10.1021/la400921h | Langmuir 2013, 29, 8665–8674

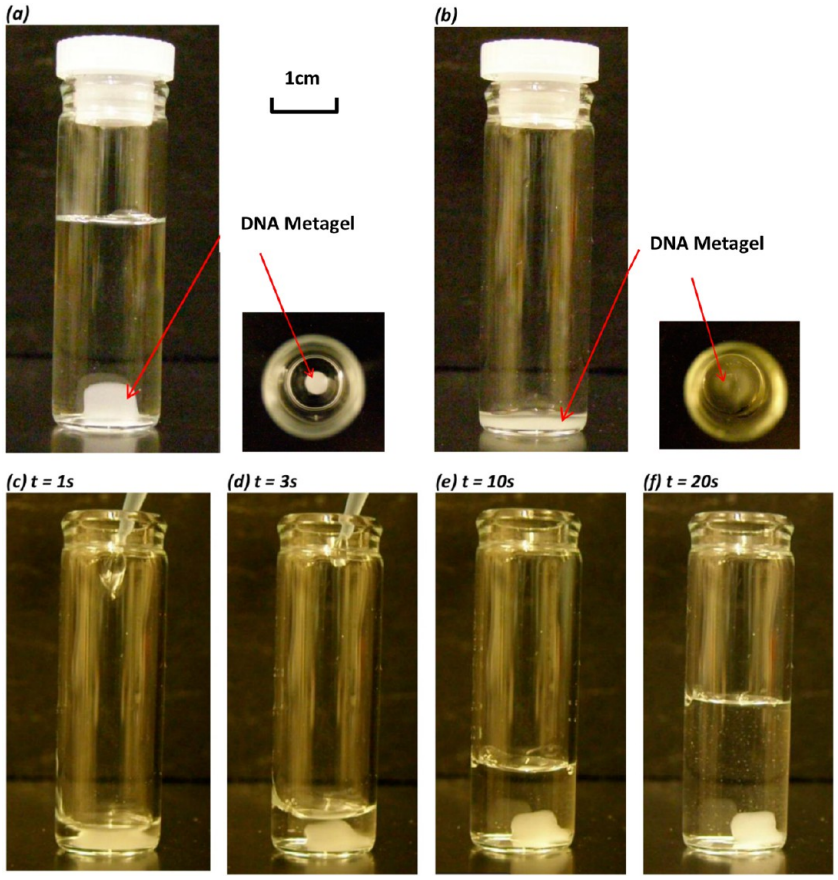

Figure 1. Shape Change of a DNA Metahydrogel Cylinder. (a) Side and top views of a cylindrically shaped hydrogel placed in a glass container submerged in water; (b) side and top views of the cylindrically shaped hydrogel deformation after water has been extracted within seconds; (c–f) time sequence of images of the hydrogel in b as water is reintroduced into the glass container at $t = 0$; the hydrogel recovers to its original cylindrical shape in less than 20 s. The characteristic time for the swelling of the gel sample is on the order of hours; hence the shape recovery is due to the elasticity of the hydrogel network.

Perhaps the most familiar phenomenon that demonstrates surface tension in liquids is the shape of a pendant drop,[13] which the theory of capillary allows us to compute in terms of two forces: gravity and surface tension. As a solid becomes increasingly compliant, a natural question arises: how do gravity and surface tension control the shape of soft materials? That is the subject of this Article.

2. DEFORMATION MAP

Because a liquid has no natural configuration, the shape of a liquid drop in contact with a solid substrate is determined by its volume and the energies of the three interfaces: liquid–vapor, solid–liquid, and solid–vapor. The equilibrium shape is the one that minimizes the free energy, which has contributions only from surface energy terms. For a solid, however compliant, one must additionally specify a reference unstressed configuration for the body as well as the elastic properties of the solid. In this Article, we assume that our soft solid is incompressible, isotropic, and hyperelastic. The assumption of hyperelasticity implies the existence of a strain energy density function W and allows for an arbitrarily large deformation. The strain energy density W of an isotropic incompressible material has the form[14]

$$W = \mu\varphi(I_1, I_2) \tag{1}$$

where φ is a dimensionless function of its dimensionless arguments I_1 and I_2, which are scalar invariants of the deformation gradient tensor, and μ is the small strain shear modulus. Specifically,

$$I_1 = \sum_{i=1}^{3} \lambda_i^2, \qquad I_2 = \lambda_1^2\lambda_2^2 + \lambda_1^2\lambda_3^2 + \lambda_2^2\lambda_3^2 \tag{2}$$

where the λ_i's are the principal stretch ratios. The simplest example is an ideal rubber or a neo-Hookean solid, where

$$\phi(I_1, I_2) = \frac{\mu(I_1 - 3)}{2} \tag{3}$$

In the following text, for simplicity we shall assume that the dimension of our soft material is characterized by d. For example, the solid can be a sphere of radius d, a cube with sides d, or a long slab with height d. Let γ denote the surface tension of the soft solid and let ρ denote its mass density. Imagine that the solid is formed by pouring a liquid into a mold followed by its gelation or cross-linking into a solid. The reference configuration of the soft material is determined by the geometry of the solid in the mold. For the sake of argument, let us consider a cube with sides d. In applications, it is important to determine its shape after release from the mold. If d is very small, then the deformation is expected to be predominantly driven by the surface tension because the

dx.doi.org/10.1021/la400921h | Langmuir 2013, 29, 8665–8674

average strain of the cube due to surface tension is on the order of

$$\alpha \equiv \frac{\gamma}{\mu d} \tag{4}$$

However, if the cube is sufficiently large, then gravity will dominate, in which case the average strain will be on the order of

$$\beta \equiv \frac{\rho g d}{\mu} \tag{5}$$

where g is the acceleration of gravity.

The dominant forces that drive the deformation can be determined by comparing the magnitude of the two dimensionless strain parameters α and β to each other and to unity. The influence of gravity and surface tension is about the same when the cube has sides of the characteristic length scale d_c determined by the condition

$$\frac{\rho g d_c}{\mu} = \frac{\gamma}{\mu d_c} \tag{6}$$

Equation 6 can expressed in terms of the Bond or Eötvös number $b_o \equiv \rho g d^2/\gamma$,

$$b_o(d_c) = \frac{\rho g {d_c}^2}{\gamma} = 1 \tag{7}$$

That is, gravity dominates deformation for large Bond numbers and surface tension drives deformation for small Bond numbers.

Equation 7 shows that d_c is independent of the modulus. For materials such as hydrogels with a surface energy and density similar to those of water, the characteristic length scale d_c is on the order of 3 mm. In this regime, a rough estimate of the magnitude of the average strain in a meta-gel cube, using μ = 6 Pa, shows that $\gamma/\mu d_c$ = 4, which corresponds to an average strain of 400%. However, if the same cube was made of PDMS, the average strain would be smaller by a factor of 10^6 because the shear modulus of PDMS is about 1 MPa and its surface tension is about 20 mJ m^{-2}.

The fact that deformation depends on two dimensionless "average strain" parameters α and β suggests the use of a 2D deformation map (Figure 2) in the space spanned by these variables, which shows how shape changes depend on them. Specifically, we introduce a strain space with coordinates (α, β). Each point in this space corresponds to the shape of a given (initially stress-free) elastic body deformed by a combination of gravity and surface tension. The origin (0, 0) corresponds to the initial shape. It is convenient in this strain space to use a polar system of coordinates (R, θ) related to the strain parameters by

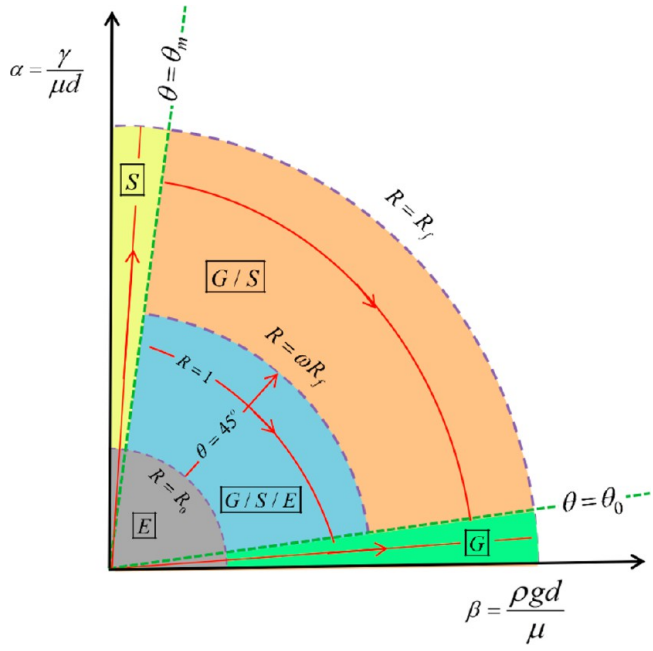

Figure 2. Deformation map. We describe five regions according to the relative importance of the roles of elasticity, surface tension, and gravity in defining the shape of a soft material: (1) small strain regime (E), (2) gravity-dominant regime (G), (3) surface tension dominant regime (S), (4) gravity and surface tension dual action regime (G/S), and (5) gravity, surface tension, and elasticity triple-action regime (G/S/E). An analysis has been carried out for each regime along the red paths.

$$\alpha = \frac{\gamma}{\mu d} = R \sin\theta$$

$$\beta = \frac{\rho g d}{\mu} = R \cos\theta$$

where

$$\begin{cases} \tan\theta = \dfrac{\gamma}{\rho g d^2} = \dfrac{1}{b_o} \\ R = \sqrt{\alpha^2 + \beta^2} = \dfrac{1}{\mu}\sqrt{\left(\dfrac{\gamma}{d}\right)^2 + (\rho g d)^2} \end{cases} \tag{8}$$

Circular arcs in the deformation map correspond to a changing Bond number b_o with a constant elastic modulus, whereas the elastic modulus decreases with increasing distance along a radial line. Thus, R is a measure of strains due to surface tension and gravity; a point at a distance far away from the origin corresponds to very large shape change.

Dashed and dotted lines in Figure 2 divide the deformation map into five regimes. The gray regime (E) occupies the interior of a small quartered circle of radius $R_0 \ll 1$ centered at the origin, where R_0 is some value small enough compared to unity for strain to be regarded as negligible. In this region, the deformation due to gravity and surface tension is negligibly small. This is the typical situation for structures made of stiff materials such as ceramics, metals, and inorganic glasses for any value of d greater than a few atomic spacings. The other extreme of $R \to \infty$ is clearly impossible because no solid can support infinite deformation, so there must exist a circle of radius R_f outside of which the solid fails. We need only to consider points inside this circle. If we pick some suitably small

dx.doi.org/10.1021/la400921h | Langmuir 2013, 29, 8665−8674

value of $\theta_0 \ll 1$, then the circular sector bounded by $0 \le \theta \le \theta_0$ and $R < R_f$ represents the green regime (G), where gravity is the dominant force that drives deformation. Similarly, the yellow regime (S) is the circular sector bounded by $\theta_m \le \theta \le \pi/2$ and $R < R_f$, where a value of θ_m suitably close to $\pi/2$ is chosen such that surface tension dominates. The region in between regimes E, G, and S can further be separated into two regimes. One of them, the blue regime (G/S/E), is bounded by $0 < \theta < \pi/2$ and $R \le \omega R_f$, where $\omega < 1$ is a positive number that characterizes the maximum deformation allowed by which this regime is defined. Inside this region, the deformed shape is driven by both gravity and surface tension, and shape change is resisted by the restoring forces of elasticity. Finally, in the orange regime (G/S), $0 < \theta < \pi/2$ and $R > \omega R_f$, the modulus is sufficiently small that the material behaves almost like a liquid. As a result, the final deformed shape bears little resemblance to the original shape. For example, a cube and a long cylindrical bar of the same volume can be deformed into a sphere of the same radius. It is clear that these regimes do not have clear-cut boundaries; for example, we can set $\omega = 3/4$.

Such a deformation map would apply to freely suspended and roughly equiaxial stress-free shapes (cubes, spheres, etc.). Specifically, the deformation map does not account for the effect of boundary conditions imposed on the deformation of the elastic body. The analogous situation for liquid capillarity is the difference between the shapes of a pendant drop and a drop of the same liquid in contact with a solid surface. As expected, the shape change will also be affected by the contact condition, which is determined by friction, adhesion, and the affinity (or lack thereof) of the surfaces in contact. This will be discussed in more detail below.

3. EXAMPLE OF A DEFORMATION MAP

As a concrete example, in the following text we will determine the shape change of an initially stress-free circular cylinder with equal height and diameter d as shown schematically in Figure 3,

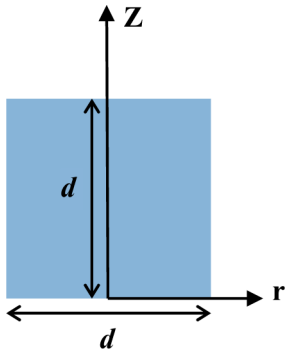

Figure 3. Referential undeformed configuration. We use a short circular cylinder with equal height and diameter in all simulations.

where Z and r denote the vertical and radial positions of a material point in the referential undeformed configuration, respectively. After the cylinder is released from the mold in which it was cast, it is placed on a flat frictionless rigid surface and is deformed by gravity and surface tension.

Determining the shape change of 3D elastic bodies with an arbitrary initial shape due to surface tension and gravity is a nontrivial problem. In this work, we consider only axisymmetric deformation. Consistent with this assumption, surfaces in this study are assumed to be homogeneous and isotropic so that surface stress is an isotropic tensor with magnitude equal to the surface tension. We avoid elastic instabilities such as buckling by restricting our attention to a short cylinder. (See the Conclusions and Discussion section.) However, the governing equations of elasticity are still nonlinear as a result of the nonlinear kinematics caused by large deformation as well as nonlinear material behavior. Additional nonlinearity is also introduced by the shape changes and the contact condition. Specifically, the location of the contact line, which in our case is a circle, is unknown and dependent on boundary or contact conditions. As in most contact mechanics approaches, we assume frictionless contact. For hydrogels, it is also reasonable to assume the interfacial tension of the gel(g)/air(v) interface, γ_{gv}, to be the surface tension of water. Because a solid (e.g., gel) can resist shear, the contact angle ϕ between the solid and the substrate is determined numerically by solving the full set of elasticity equations and in general does not satisfy Young's equation[15]

$$\cos\phi = \frac{\gamma_{sv} - \gamma_{sg}}{\gamma_{gv}} \tag{9}$$

where γ_{sv} and γ_{sg} are the interfacial energies between the substrate (s)/air (v) and substrate (s)/gel (g), respectively. There is but one exception for the examples in this work: $\phi = \pi/2$ if $\gamma_{sv} = \gamma_{sg}$; this is because the substrate is rigid and the undeformed cylinder's lateral surface is perpendicular to the substrate. In general, even though the contact angle may not be given by eq 9, it is expected that the contact angle will be more than $\pi/2$ if $\gamma_{sv} - \gamma_{sg} < 0$ and less than $\pi/2$ if $\gamma_{sv} - \gamma_{sg} > 0$. In this paper, we neglect adhesion—the position of the contact line is determined by the (Hertz) condition. It lies where the normal interfacial traction between the cylinder and the substrate turns purely compressive. The role of adhesion will be discussed in the last section of this Article.

Although there is no difficulty in using more sophisticated models to quantify material behavior, we use the neo-Hookean model so as to capture large deformation while retaining the simplicity of a single parameter (μ) to represent elasticity. A finite element method (FEM) is used to solve for the deformation and stresses caused by gravity and surface tension. Commercial software ABAQUS is used in all of our numerical simulations. Loading due to surface tension is simulated via a user-defined surface element.[1,16] Details of our finite element method are given in the Supporting Information. In the following text, we will present the numerical results. Approximated analytical solutions are possible in regimes 2, 3, and 4, and we will compare these solutions to our FEM results.

4. RESULTS

4.1. Regime E: Small Strain Regime $\alpha \ll 1$ and $\beta \ll 1$.

In this regime, the stress−strain relation of an isotropic hyperelastic material in the infinitesimal strain limit reduces to isotropic linear elasticity. Surface tension and gravity effects can be neglected.

4.2. Regime G: Gravity-Dominant Regime $\alpha \ll \beta$ and $\alpha \ll 1$.

Gravity dominantly drives the deformations of solids in this regime, whereas surface tension acts only locally to round off sharp edges. Hence, the deformation in this regime is controlled solely by the strain parameter $\beta \equiv \rho g d/\mu$.

We carried out our analysis along the red line in regime G of the deformation map shown in Figure 2. An approximate

dx.doi.org/10.1021/la400921h | Langmuir 2013, 29, 8665−8674

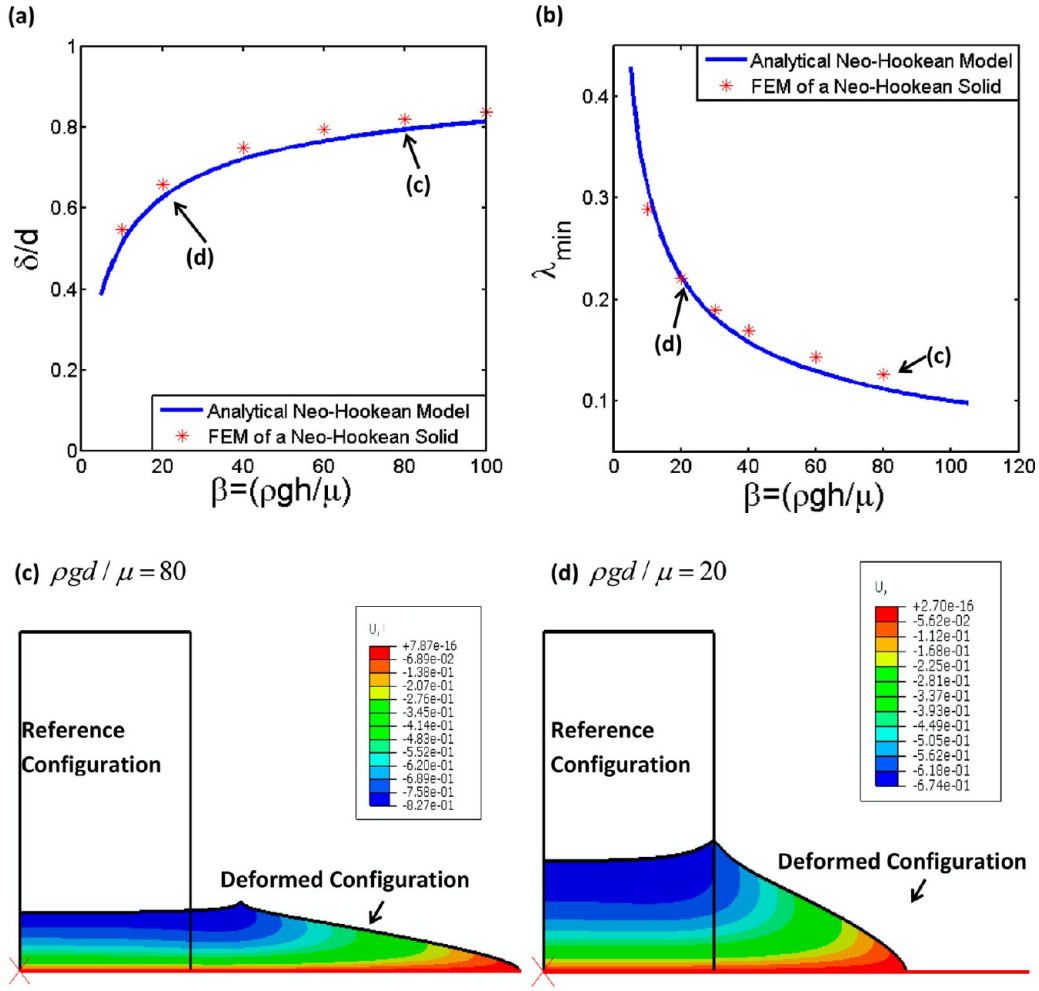

Figure 4. Results for the gravity-dominant regime using a neo-Hookean model. (a) (Average) vertical displacement at the top surface δ/d against β. (b) Minimum stretch ratio λ_{min} (average vertical stretch ratio at the bottom surface) against β. (c) Initial and deformed shapes at β = 80. (d) Initial and deformed shapes at β = 20. Contours represent surfaces of constant vertical displacement U_2.

analytical large-strain solution can be obtained by assuming that all of the components of the first Piola−Kirchhoff stress vanish except the one that is parallel to the direction of gravity (i.e., Z direction in the referential configuration shown in Figure 3). A straightforward analysis shows that the stretch ratio in vertical direction $\lambda_Z \equiv \lambda$ is related to Z in the reference configuration by

$$\lambda - \frac{1}{\lambda^2} = \beta(z-1), \quad \text{where} \quad \beta = \frac{\rho g d}{\mu}, z = \frac{Z}{d} \tag{10}$$

Equation 10 has only one positive real root of λ, whose value depends on the discriminant $\Delta = 4\beta^3(1-z)^3 - 27$:

$$\begin{aligned}
&\Delta = 0,\ \lambda = 2^{-2/3}\\
&\Delta < 0,\ \lambda = -\frac{1}{3}\left\{\beta - \beta z \right.\\
&\quad + \sqrt[3]{\frac{1}{2}(2\beta^3(1-z)^3 - 27 + \sqrt{-27\Delta})}\\
&\quad \left. + \sqrt[3]{\frac{1}{2}(2\beta^3(1-z)^3 - 27 - \sqrt{-27\Delta})}\right\}\\
&\Delta > 0,\ \lambda = \frac{2\beta(1-z)}{3}\cos\left(\frac{n+m\pi}{3}\right) - \frac{\beta(1-z)}{3}\\
&\quad \text{where} \quad m = 0, 2, 4,\ n = \cos^{-1}\left(\frac{27 - 2\beta^3(1-z)^3}{2\beta^3(1-z)^3}\right)
\end{aligned} \tag{11}$$

The vertical displacement δ of the top free surface normalized by the initial height of the cylinder, d, can be obtained using

$$\frac{\delta}{d} = 1 - \int_0^1 \lambda(\beta, z)\, \mathrm{d}z \tag{12}$$

Another quantity of interest is the minimum stretch ratio λ_{min} ($\lambda_{min} < 1$ indicates that material element is compressed), which occurs at the bottom surface (i.e., z = 0). Because the approximated analytical solution assumes the deformation of a point being independent of its lateral position, we compare the results from eqs 11 and 12 with numerical results by taking the average of top surface (bottom surface) vertical displacements (stretch ratios) from the FEM simulation.

Figure 4a plots the (average) vertical displacement at the top surface against strain parameter β. Figure 4b shows the variation in λ_{min} with β. The analytical solution is found to be in good agreement with the FEM result. The deformed shape is compared to the initial shape in Figure 4c,d for β = 80 and 20. Because of symmetry, only half of the cylinder is shown with contours representing surfaces of constant vertical displacement U_2.

The DNA hydrogel sample in Figure 1 lies approximately in this regime. A rough estimate of the magnitude of average

dx.doi.org/10.1021/la400921h | Langmuir 2013, 29, 8665−8674

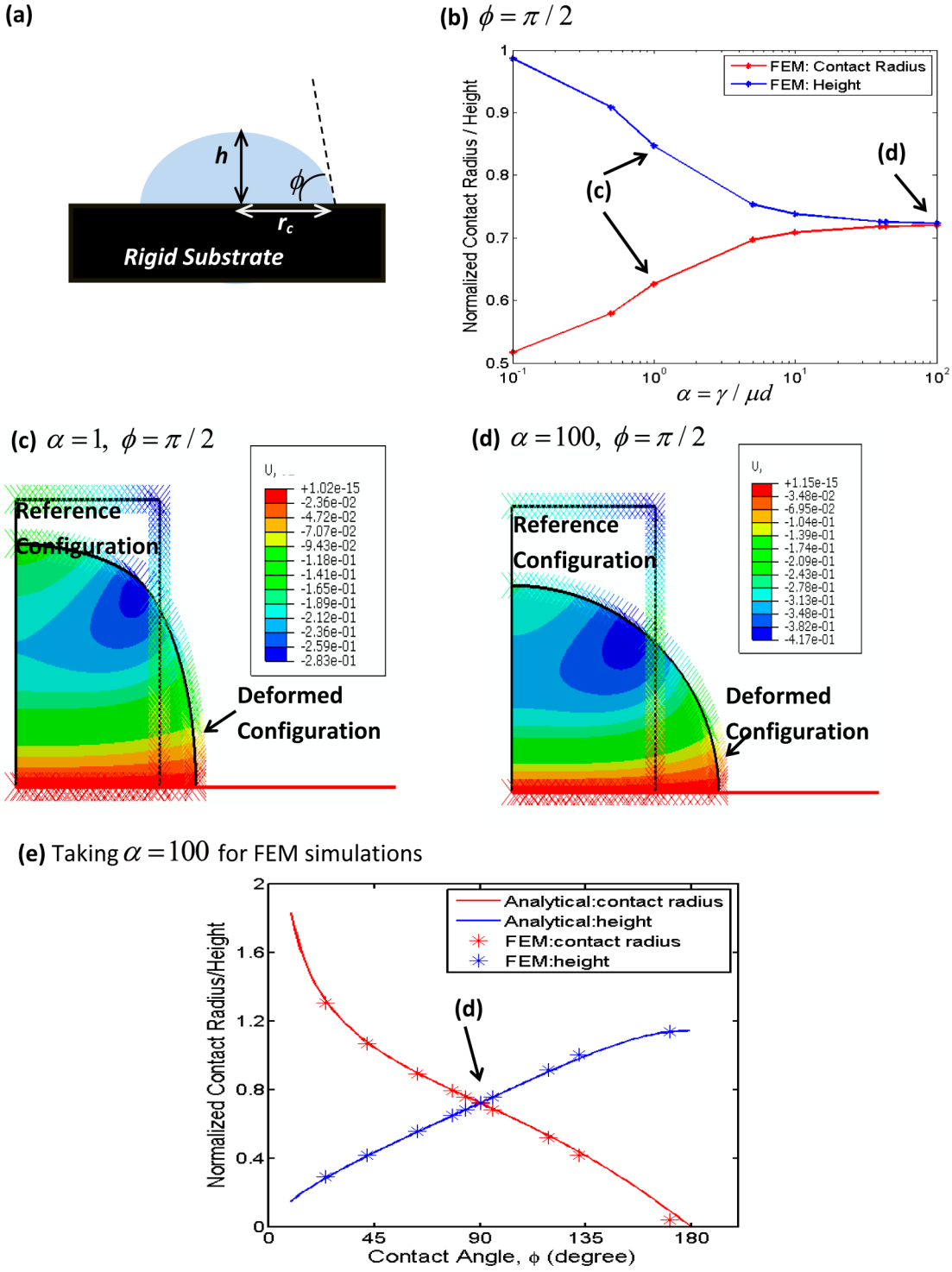

Figure 5. Results for the surface tension dominant regime. (a) Deformed configuration. (b) Plots of normalized contact radius r_c and deformed height h against strain parameter α for contact angle $\phi = \pi/2$. (c) Comparison of deformed shape with initial shape for $\alpha = 1$, $\phi = \pi/2$. (d) Comparison of deformed shape with initial shape for $\alpha = 100$, $\phi = \pi/2$. (e) Plots of r_c and h against contact angle ϕ when $\alpha \gg 1$; FEM results are obtained at $\alpha = 100$.

strains in the gel sample, using $\mu = 5$ Pa, gives $\alpha \approx 2$ and $\beta \approx 15$. Figure 1 shows that the gravity force compressed the sample to less than half of its initial height. It agrees qualitatively with our numerical results.

4.3. Regime S: Surface Tension Dominant Regime $\alpha \gg \beta$ and $\beta \ll 1$. The average strain due to gravity is small for solids in this regime, so we can characterize the deformation based solely on the strain parameter $\alpha = \gamma/\mu d$. The effect of surface tension becomes increasingly prominent as one moves along the red line in the direction of increasing α on the deformation map (regime S) in Figure 2. When $\alpha \gg 1$ (i.e., structures of very small size or materials with negligible modulus) is reached, the surface tension deforms solids into spherical caps, regardless of their initial shape.

dx.doi.org/10.1021/la400921h | Langmuir 2013, 29, 8665−8674

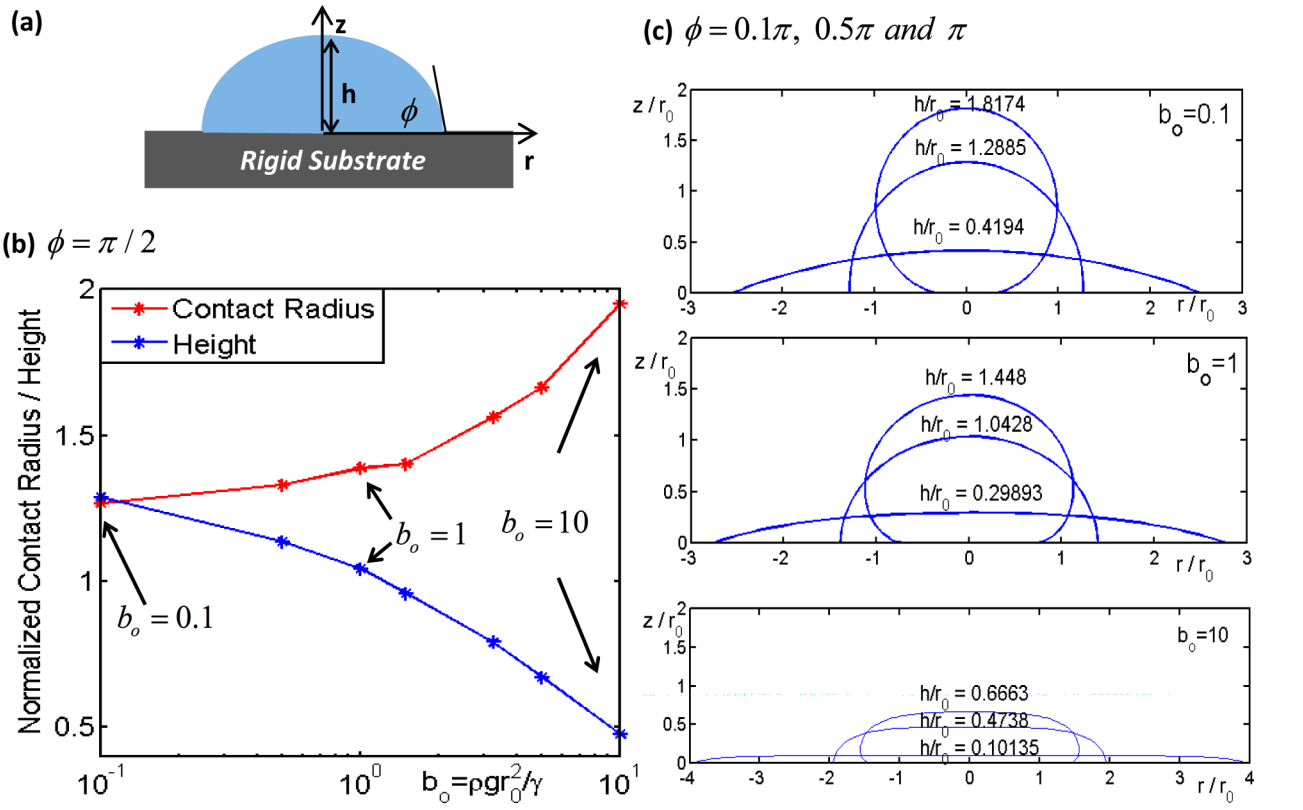

Figure 6. Results for gravity and surface tension dual action regime. All lengths are normalized by r_0: (a) deformed configuration; (b) plots of contact radius r_c and deformed height h against Bond number with contact angle $\pi/2$; (c) deformed shapes plotted for contact angles of $\pi/10$, $\pi/2$, and π at given Bond numbers of 0.1, 1, and 10.

In the following text, we characterize the deformed shapes using the deformed height h and the contact base radius r_c as defined in Figure 5a, and all length scales are normalized by the initial height d of the cylinder. First, we consider the special case where the contact angle is $\phi = \pi/2$. Results from FEM simulations for increasing values of α are plotted in Figure 5b for this case. As expected, the deformed height h and the contact base radius r_c converge to the same value as α increases, implying that the deformed shape is a hemisphere. Figure 5c,d compares the deformed shapes with the initial shape for $\alpha = 1$ and 100, respectively, with prescribed contact angle $\phi = \pi/2$. For $\alpha = 1$ (Figure 5c), the surface tension effect is confined to the corner (i.e., the top edge of the cylinder), and the rest of the original shape is mostly unchanged because of resistance by elasticity. In contrast, for $\alpha = 100$ (Figure 5d), surface tension dominates elasticity and the deformed shape is approximately a hemisphere.

To validate our FEM results further, we note that an analytical solution can be obtained for the special case of $\alpha \gg 1$. In this regime, the final deformed shape is a spherical cap and is approximately independent of the initial shape. Because the material is incompressible, the dimensions of the spherical cap are completely determined by the initial volume of the solid V_0 and the equilibrium contact angle ϕ. Specifically, the height of the cap h and the radius of its base r_c are obtained by solving eqs 13 and 14,

$$\cos\phi = \frac{r_c^2 - h^2}{r_c^2 + h^2} \tag{13}$$

$$V_0 = \frac{\pi}{6} h(3r_c^2 + h^2) \tag{14}$$

Figure 5b shows that the spherical cap solution given by eqs 13 and 14 is a good approximation when α is greater than 10. Hence in Figure 5e we compare the FEM results for $\alpha = 100$ to the analytical results for the full range of contact angles. In this figure, the volume of the cylinder $V_0 = (\pi d^3)/4$ is fixed. The results show good agreement between the approximated theory and FEM simulations.

4.4. Regime G/S: Gravity and Surface Tension Dual Action Regime $\alpha \gg 1$ and $\beta \gg 1$. Solids in this regime deforms like a liquid with no apparent resistance to shape change because gravity, surface tension, or both overwhelm the elastic restoring forces. In this regime, the deformed shape is dependent only on the initial volume V_0 (which remains constant because of incompressibility), boundary conditions (we assume frictionless contact and prescribe the contact angle ϕ), and the Bond number b_o; it is approximately independent of the initial shape. Hence the deformed shape is governed by the standard theory of liquid capillarity, but as demonstrated in Figure 1, the solid can still retain its ability to recover its original shape if gravity and surface tension are removed. For an axisymmetric liquid drop in a gravity field,[17] the final deformed shape can be determined by solving a boundary value problem involving three ordinary differential equations. Because the theory is well known, we include the relevant details in the Supporting Information; here we present the results of these calculations.

The deformed coordinates in these calculations are defined in Figure 6a. It is convenient to normalize all length scales by r_0, the radius of a sphere with the same volume V_0 as the

dx.doi.org/10.1021/la400921h | Langmuir 2013, 29, 8665−8674

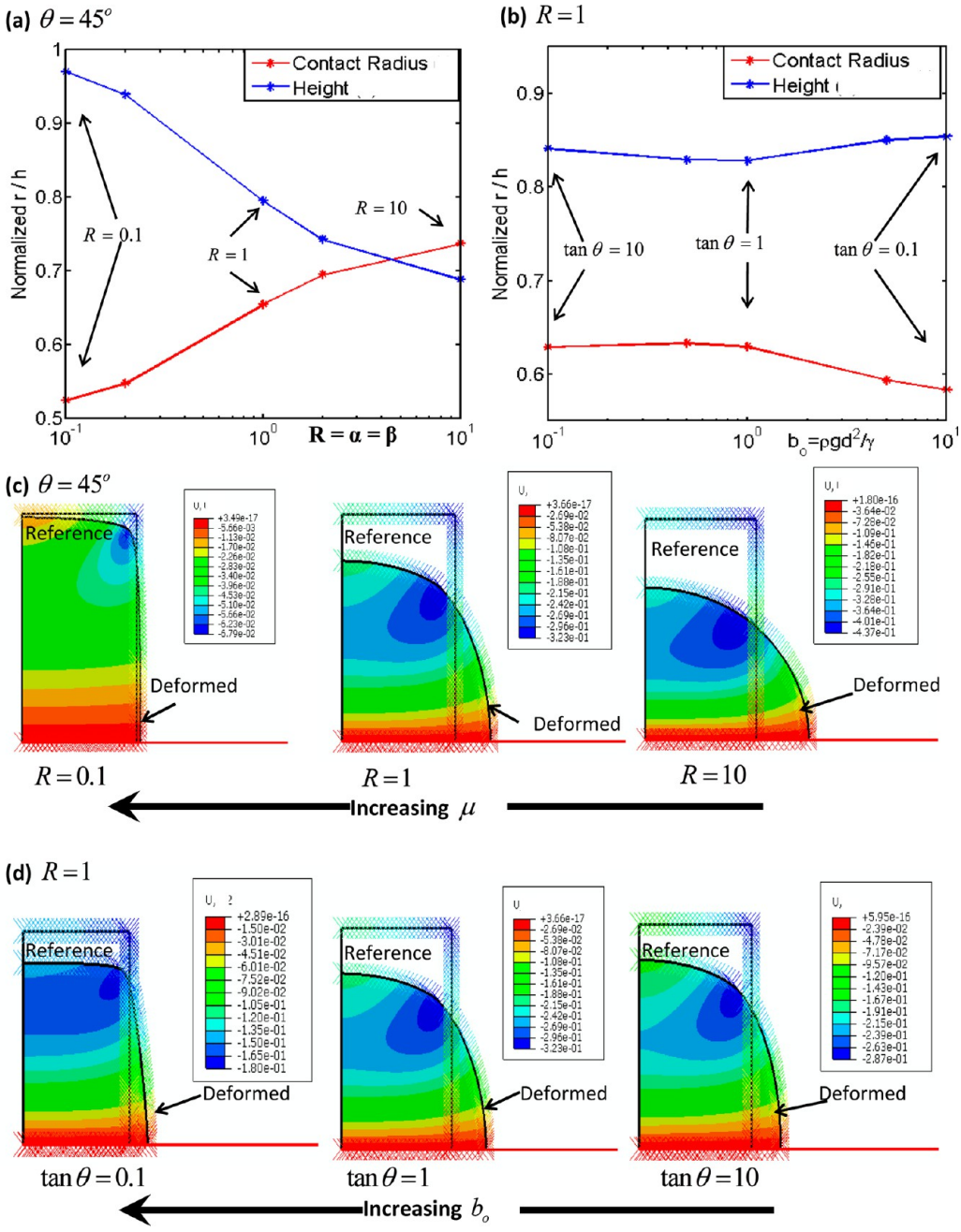

Figure 7. Results for the gravity, surface tension, and elasticity triple-action regime. All lengths are normalized by the initial height of the cylinder d: (a) Plots of contact radius r_c and deformed height h along the radial line on the deformation map of $\theta = 45°$. (b) Plots of r_c and h along the arc of $R = 1$ on the deformation map. (c) Deformed shapes corresponding to points labeled in plot a are compared to the initial shape. (d) Deformed shapes corresponding to points labeled in plot b are compared to the initial shape. Colors denote contours of constant vertical displacement $U2$.

undeformed solid. We start by prescribing the contact angle to be $\pi/2$ and vary the Bond number so that these deformations lie on the circular arc in regime 4 of the deformation map in Figure 2. When the Bond number is small ($b_o = 0.1$), surface tension outweighs gravity and the deformed shape can be approximated by a hemisphere (i.e., $r_c \approx h$ as shown in Figure 6b). As the gravity becomes more significant with increasing b_o, the contact radius and deformed height diverge from each other, indicating that the solid is crushed into the shape of a pancake (similar to the situation in Figure 1).

For a given contact angle, the contact radius and deformed height as well as the deformed shape can be completely determined for a given Bond number as illustrated in Figure 6c. Results for different Bond numbers, 0.1, 1, and 10, are shown in three plots. Each plot shows the deformed shapes of the contact angle ϕ prescribed to be 0.1π, 0.5π, and π.

4.5. Regime G/S/E: Gravity, Surface Tension and Elasticity Triple Action Regime. Finally, in the last regime, where the elastic modulus of the solid is no longer negligible and the gravity and surface tension effects are comparable to each other, we carry out two series of finite element simulations: one is along the radial line labeled $\theta = 45°$ (or $b_o = 1$, where surface tension and gravity effects are comparable), and the other is along the arc labeled $R = 1$ in the deformation map (where the average strain is 100%). All

dx.doi.org/10.1021/la400921h | Langmuir 2013, 29, 8665−8674

simulations are based on a contact angle of $\phi = \pi/2$, and we normalize all lengths by the initial height of the cylinder d.

For the first series of simulations along $\theta = 45°$, the radial distance R on the deformation map increases with decreasing shear modulus μ while the Bond number is fixed at 1. The contact radius r_c and deformed height h are plotted against the average strain R in Figure 7a. As expected, the deformed height decreases and the contact radius increases with increasing average strain R. Deformed shapes for the cases of $R = 0.1$, 1, and 10 (indicated by arrows in Figure 7a) are compared to the initial shape in Figure 7c.

Figure 7b plots results from the second series of simulations where the average strain R is fixed to be 1 while the Bond number changes. An increase in the Bond number (i.e., a decrease in θ on the deformation map) indicates the increasing importance of gravity compared to that of surface tension. Figure 7b shows that the contact radius and deformed height are quite insensitive to the Bond number for a given average deformation R. Selected deformed shapes of the cases $\tan\theta = 0.1$, 1, and 10 are also compared to the reference configuration in Figure 7d corresponding to points labeled in Figure 7b. Colors in these figures denote contours of constant vertical displacement $U2$.

5. CONCLUSIONS AND DISCUSSION

A deformation map is proposed to characterize the shape change of soft materials subjected to gravity and surface tension forces. The deformation map can be partitioned into five regimes, and the characteristic of each regime is described in some detail using a specific example of a short circular elastic cylinder placed on a flat, smooth rigid substrate. A circular cylinder is chosen in this work, but there is no difficulty simulating other geometries. It has long been known that a long elastic column will buckle under its own weight when its length exceeds $L_{max} = (7.84w/D)^{1/3}$, where w is the weight per unit length and D is the flexural rigidity of the column.[18] Hence we study the deformation of a short cylinder to avoid nonunique solutions caused by buckling. Experimental data of the cylindrical DNA hydrogel sample in Figure 1 is also compared qualitatively to our numerical results in the gravity-dominant regime.

In our analysis, we assume the soft material is incompressible, isotropic, and neo-Hookean. This is the simplest material model that captures many important features of elastic materials composed of polymer networks. It is well known that the neo-Hookean model underestimates the amount of strain hardening, especially in the large deformation regime when chains between cross links are fully extended. Hence our solution tends to overestimate the amount of deformation. The calculations and simulations in this work can be readily extended to other strain-energy functions that model these strain-hardening effects as well as anisotropy and compressibility. Because these models are material-specific, we leave these applications to future work.

An accurate representation of the contact requires a quantitative description of surface interactions. Modeling realistic surface interactions is still an unresolved problem. There is no universally accepted model that accounts for both friction and adhesion, not to mention hydrophobic and hydrophilic interactions. In all of our simulations, a frictionless boundary condition is enforced, which is an assumption that is consistent with most contact mechanics approaches. Undoubtedly, there are situations where the frictionless boundary condition is inappropriate. However, there is no difficulty enforcing the opposite limit where no slip is allowed in our simulations.

A final word regarding the use of the frictionless boundary condition: on a frictionless interface, the contact line is free to move laterally so that quantities γ_{sv} and γ_{sg} in Young's eq 9 should be interpreted as interfacial energies and not as interfacial tensions. However, if no slip is allowed, these quantities should be regarded as interfacial tensions. This distinction is important because the surface energy of a solid can be different from its surface tension.

We emphasize that there are two distinct approaches to the contact mechanics of liquid drops and elastic bodies. In the literature, the equilibrium shape of a liquid drop on a frictionless rigid substrate is determined by Young's equation and the Laplace capillary equation. However, the shape of an elastic solid in contact with a rigid substrate is determined by solving the full elasticity equations subjected to displacement and traction continuity in the contact region without regard for interfacial energies and surface tension. The location of the contact line is determined by enforcing the Hertz condition for adhesionless contact. (That is, only compression is allowed inside the contact region, and it is traction-free outside.) Adhesion can be accounted for using cohesive zone models that specify how interfacial traction varies with interfacial displacements.[19] These two approaches are distinct and cannot be reconciled without additional physics because they are based on different sets of equations. Our formulation unifies these two approaches because the surface of our elastic solid is endowed with surface tension elements so that our results will approach the capillary limit when the shear modulus of our elastic solid approaches zero. In our simulations, we assume adhesionless contact to reduce the number of material parameters. Adhesion is clearly important when structural dimensions or moduli are small, that is, in the surface-tension-dominated regime. The effect of adhesion can be modeled by incorporating surface interaction potentials and will be addressed in future work.

■ ASSOCIATED CONTENT

Supporting Information

Detailed analytical calculations in the gravity regime and gravity and surface tension dual-action regime. Details of FEM simulations of the surface tension effect. This material is available free of charge via the Internet at http://pubs.acs.org

■ AUTHOR INFORMATION

Notes

The authors declare no competing financial interest.

■ ACKNOWLEDGMENTS

C.-Y.H., A.J., and X.X. acknowledge support from the U.S. Department of Energy, Office of Basic Energy Science, Division of Material Sciences and Engineering under award DE-FG02-07ER46463.

■ REFERENCES

(1) Hui, C. Y.; Jagota, A.; Lin, Y. Y.; Kramer, E. J. Constraints on Microcontact Printing Imposed by Stamp Deformation. *Langmuir* **2002**, *18*, 1394−1407.

(2) McDonald, J. C.; Whitesides, G. M. Poly(dimethylsiloxane) as a Material for Fabricating Microfluidic Devices. *Acc. Chem. Res.* **2001**, *35*, 491−499.

(3) Jagota, A.; Hui, C. Y. Adhesion, Friction, and Compliance of Bio-Mimetic and Bio-Inspired Structured Interfaces. *Mater. Sci. Eng.: Rep.* **2011**, *72*, 253−292.
(4) Hoffman, A. S. Hydrogels for Biomedical Applications. *Adv. Drug Delivery Rev.* **2012**, *64* Supplement, 18−23.
(5) Lee, J. B.; Peng, S.; Yang, D.; Roh, Y. H.; Funabashi, H.; Park, N.; Rice, E. J.; Chen, L.; Long, R.; Wu, M.; Luo, D. A Mechanical Metamaterial Made from a DNA Hydrogel. *Nat. Nanotechnol.* **2012**, *7*, 816−820.
(6) Gibbs, J. On the Equilibrium of Heterogeneous Substances. *Trans. Conn. Acad.* **1876**, *3*, 343−524.
(7) Jagota, A., P. D. . G. A. Surface-Tension-Induced Flattening of a Nearly Plane Elastic Solid. *Phys. Rev. E* **2012**, *85*, 051602.
(8) Roman, B.; Bico, J. Elasto-Capillarity: Deforming an Elastic Structure with a Liquid Droplet. *J. Phys.: Condens. Matter* **2010**, *22*, 493101.
(9) Yu, Y.-s. Substrate Elastic Deformation Due to Vertical Component of Liquid-Vapor Interfacial Tension. *J. Appl. Math. Mech. (Engl. Transl.)* **2012**, *33*, 1095−1114.
(10) Style, R. W.; Che, Y.; Wettlaufer, J. S.; Wilen, L.; Dufresne, E. R. Universal Deformation of Soft Substrates Near a Contact Line and the Direct Measurement of Solid Surface Stresses. *Phys. Rev. Lett.* **2013**, *110*, 066103.
(11) Jerison, E. R.; Xu, Y.; Wilen, L. A.; Dufresne, R. The Deformation of an Elastic Substrate by a Three-Phase Contact Line. *Phys. Rev. Lett.* **2011**, *106*, 186103.
(12) Mora, S.; Phou, T.; Fromental, J.-M.; Pismen, L. M.; Pomeau, Y. Capillarity Driven Instability of a Soft Solid. *Phys. Rev. Lett.* **2010**, *105*, 214301.
(13) deGennes, P. G.; Brochard-Wyart, F.; Quere, D. *Capillarity and Wetting Phenomena: Drops, Bubbles, Pearls, Waves*; Springer: New York, 2002.
(14) Rivlin, R. S. Large Elastic Deformations of Isotropic Materials. IV. Further Developments of the General Theory. *Philos. Trans. R. Soc. London, Sect. A* **1948**, *241*, 379−397.
(15) Young, T. An Essay on the Cohesion of Fluids. *Philos. Trans. R. Soc. London* **1805**, *95*, 65−87.
(16) Jagota, A.; Argento, C.; Mazur, S. Growth of Adhesive Contacts for Maxwell Viscoelastic Spheres. *J. Appl. Phys.* **1998**, *83*, 250−259.
(17) Adamson, A. W.; Gast, A. P. *Physical Chemistry of Surfaces*; Wiley: New York, 1997.
(18) Greenhill, A. G. Determination of the Greatest Height Consistent with Stability That a Vertical Pole or Mast Can Be Made, And the Greatest Height to Which a Tree of Given Proportions Can Grow. *Proc. Cambridge Philos. Soc.* **1881**, *4*, 65−73.
(19) Maugis, D. *Contact, Adhesion and Rupture of Elastic Solids*; Springer: New York, 2000.